Supplementary Material for: 'Externally controlled magnetism and band gap in twisted bilayer graphene'

A.O. Sboychakov,[1,2] A.V. Rozhkov,[1,2,3] A.L. Rakhmanov,[1,3,2,4] and Franco Nori[1,5]

[1] *Center for Emergent Matter Science, RIKEN, Wako-shi, Saitama, 351-0198, Japan*
[2] *Institute for Theoretical and Applied Electrodynamics, Russian Academy of Sciences, Moscow, 125412 Russia*
[3] *Moscow Institute for Physics and Technology (State University), Dolgoprudnyi, 141700 Russia*
[4] *Dukhov Research Institute of Automatics, Moscow, 127055 Russia*
[5] *Department of Physics, University of Michigan, Ann Arbor, MI 48109-1040, USA*

(Dated: February 14, 2018)

In this Supplementary Material we provide additional technical details, which should help interested readers to derive Eqs. (6) and (10) of the main text. We also derive the modification of Eq. (10) for the case of strong interaction.

I. EFFECTIVE FORM OF THE INTERACTION HAMILTONIAN

In this Section, we will explain the derivation of the effective interaction Hamiltonian, Eq. (6) of the main text. Starting with the low-energy single-electron theory, our goal here is to derive an effective Hamiltonian with electron-electron interactions.

As described in the main text, the low-energy sector of the tBLG consists of four single-electron bands. Near the Dirac points, two of these bands have electron-like near-linear dispersion, and two bands have hole-like dispersion. Let us introduce the symbols $\mathfrak{e}_\mu$ ($\mathfrak{h}_\mu$), with $\mu = \pm 1$, to denote these electron (hole) bands. We also denote the energies and wave functions of these bands as $E^{\mathfrak{e},\mathfrak{h}}_{\mathbf{p}\mu}$ and $\Phi^{\mathfrak{e}\mu,\mathfrak{h}\mu}_{\mathbf{p}\mathbf{G}is}$, respectively. The single-particle part of the effective low-energy Hamiltonian then becomes

$$\hat{H}_0^{\text{eff}} = \sum_{\mathbf{p}\mu\sigma} \left[E^{\mathfrak{e}}_{\mathbf{p}\mu} \hat{\mathfrak{e}}^\dagger_{\mathbf{p}\mu\sigma} \hat{\mathfrak{e}}_{\mathbf{p}\mu\sigma} + E^{\mathfrak{h}}_{\mathbf{p}\mu} \hat{\mathfrak{h}}^\dagger_{\mathbf{p}\mu\sigma} \hat{\mathfrak{h}}_{\mathbf{p}\mu\sigma} \right], \tag{S1}$$

where $\hat{\mathfrak{e}}^\dagger_{\mathbf{p}\mu\sigma}$ and $\hat{\mathfrak{e}}_{\mathbf{p}\mu\sigma}$ ($\hat{\mathfrak{h}}^\dagger_{\mathbf{p}\mu\sigma}$ and $\hat{\mathfrak{h}}_{\mathbf{p}\mu\sigma}$) are the creation and annihilation operators of the quasiparticle in the band $\mathfrak{e}_\mu$ ($\mathfrak{h}_\mu$) with momentum $\mathbf{p}$ and spin projection σ.

At finite bias voltage, bands $\mathfrak{e}_{-1}$ and $\mathfrak{h}_{+1}$ cross the Fermi level E_F, forming a Fermi surface. For a given band the Fermi surface consists of two sheets, one is centered at $\mathbf{K}_1$ point, another is at $\mathbf{K}_2$ point. At small bias, the sheets are approximated by circles centered at the Dirac points. The radii of all four circles are identical, and equal to $q_{\text{F}}^* \propto V_b$. This fulfills the condition of the perfect Fermi surface nesting. The nesting vector is $\mathbf{q} = 0$. At stronger bias, the energy of the tBLG van Hove singularity approaches E_F. As this happens, the sheets shape experiences stronger trigonal warping. For example, in Fig. S1 it is possible to notice visually that the sheets deviate slightly from ideal circles. Formally, near Dirac point $\mathbf{K}_1$ the Fermi surface curve is given by $\mathbf{q}_F(\varphi) = q_F(\varphi)\{\cos\varphi, \sin\varphi\}$, where the function $q_F(\varphi)$ with a good accuracy can be fitted as

$$q_F(\varphi) = q_F^* + \delta q_F \cos\left[3(\varphi - \varphi_0)\right] .$$

The last term describes the trigonal warping. Trigonal warping is more pronounced for larger V_b and smaller twist angles. Near Dirac point $\mathbf{K}_2$ we should replace $\varphi \to \varphi + \pi$.

However, even in this regime, with very good accuracy, the following condition holds true: $E^{\mathfrak{e}}_{\mathbf{p}-1} = E^{\mathfrak{h}}_{\mathbf{p}+1} = E_F$. One can say that the Fermi surface is doubly degenerate: electron sheets coincide with hole sheets. Thus, despite the warping, the nesting is preserved.

Yet, a more detailed numerical analysis shows that small de-nesting between electron and hole Fermi surface sheets is present. However, in majority of superstructures and bias voltages considered the characteristic energy of this de-nesting does not exceed the value about $10^{-4}t$. For the values of the exciton gap interesting from experimental point of view, $\Delta_+ \gtrsim 10^{-2}t$, such small deviations can be disregarded. If we neglect de-nesting, the Fermi surface can be considered consisting of two doubly degenerate closed near-circular curves around Dirac points $\mathbf{K}_{1,2}$. This is one of the simplifying conditions of our formalism.

The momentum summation in Eq. (S1) is performed over the reciprocal unit cell of the superlattice. For further consideration, it is convenient to separate this region into two valleys, as shown in Fig. S1. These regions have the form of regular triangles centered at the Dirac points $\mathbf{K}_{1,2}$. For each valley, we introduce electron operators as

$$\hat{\mathfrak{e}}^w_{\mathbf{p}\mu\sigma} = \hat{\mathfrak{e}}_{\mathbf{K}_w+\mathbf{p}\mu\sigma} , \quad \hat{\mathfrak{h}}^w_{\mathbf{p}\mu\sigma} = \hat{\mathfrak{h}}_{\mathbf{K}_w+\mathbf{p}\mu\sigma} , \tag{S2}$$

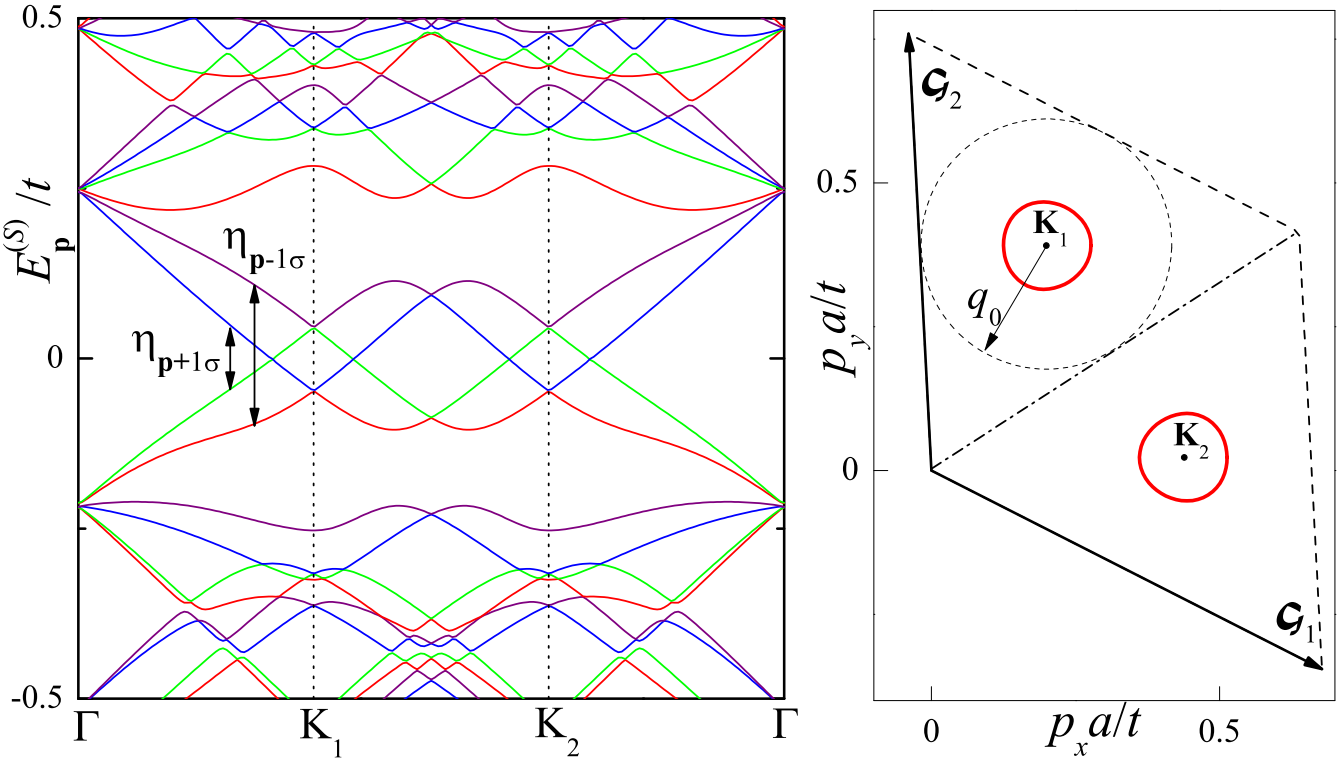

FIG. S1: (Left panel) Band structure calculated for a sample with $m_0 = 5$, $r = 1$ ($\theta \cong 6.009°$); $V_b = 0.15t$. The vertical double-arrows show the bands, which are coupled by the electron-electron interaction. (Right panel) Fermi surface corresponding to the band structure shown on the left. A slight trigonal warping of the Fermi surface curves can be seen. The dot-dashed line separates the reciprocal unit cell of the superlattice into two valleys. The dashed circle with radius q_0 is used to find an approximate solution to the gap equation in the limit of strong interaction (see the text).

where the momentum $\mathbf{p}$ is now counted from the Dirac point $\mathbf{K}_w$.

Let us now consider the interaction part of the Hamiltonian. The most general form of the interaction Hamiltonian reads

$$\hat{H}_{\rm int} = \frac{1}{2}\sum_{\substack{injm\\ ss'\sigma\sigma'}} \hat{d}^{\dagger}_{\mathbf{n}is\sigma}\,\hat{d}_{\mathbf{n}is\sigma}\,U_{ij}(\mathbf{r}^{is}_{\mathbf{n}} - \mathbf{r}^{js'}_{\mathbf{m}})\,\hat{d}^{\dagger}_{\mathbf{m}js'\sigma'}\,\hat{d}_{\mathbf{m}js'\sigma'}. \tag{S3}$$

In this equation, $\hat{d}^{\dagger}_{\mathbf{n}is\sigma}$ and $\hat{d}_{\mathbf{n}is\sigma}$ are the creation and annihilation operators of the electron with spin projection σ, located at site $\mathbf{n}$ in the layer i $(= 1, 2)$ in the sublattice s. In momentum space, we can write

$$\hat{H}_{\rm int} = \frac{1}{2\mathcal{N}}\sum_{\substack{is\sigma\\ js'\sigma'}}\sum_{\substack{\mathbf{p}_1\mathbf{p}_2\\ \mathbf{p}'_1\mathbf{p}'_2}}\sum_{\substack{\mathbf{G}_1\mathbf{G}_2\\ \mathbf{G}'_1\mathbf{G}'_2}}\sum_{\mathbf{G}} \delta_{\mathbf{G},\,\mathbf{k}_1+\mathbf{k}_2-\mathbf{k}'_1-\mathbf{k}'_2}\,\hat{d}^{\dagger}_{\mathbf{p}_1\mathbf{G}_1is\sigma}\,\hat{d}_{\mathbf{p}'_1\mathbf{G}'_1is\sigma}\,U_{is;js'}(\mathbf{k}_1-\mathbf{k}'_1;\mathbf{G})\,\hat{d}^{\dagger}_{\mathbf{p}_2\mathbf{G}_2js'\sigma'}\,\hat{d}_{\mathbf{p}'_2\mathbf{G}'_2js'\sigma'},$$

where $\mathcal{N}$ is the number of graphene unit cells in the sample in one layer, $\mathbf{k}_{1,2} = \mathbf{p}_{1,2} + \mathbf{G}_{1,2}$, $\mathbf{k}'_{1,2} = \mathbf{p}'_{1,2} + \mathbf{G}'_{1,2}$, and

$$U_{is;js'}(\mathbf{k};\mathbf{G}) = \frac{1}{N_{\rm sc}}{\sum_{\mathbf{nm}}}' \exp[-i\mathbf{k}(\mathbf{r}^{i}_{\mathbf{n}} - \mathbf{r}^{j}_{\mathbf{m}})]\exp(-i\mathbf{G}\mathbf{r}^{j}_{\mathbf{m}})U(\mathbf{r}^{is}_{\mathbf{n}} - \mathbf{r}^{js'}_{\mathbf{m}})\,. \tag{S4}$$

In the equation above, the symbol of summation with prime means that the summation over $\mathbf{m}$ is performed over sites inside the zeroth supercell, while the summation over $\mathbf{n}$ is performed over all sites in the sample. Because of the superlattice, interaction Eq. (S4) depends on two momenta, $\mathbf{k}$ and $\mathbf{G}$. This is unlike the interaction in free space, which depends on a single momentum variable. In the function $U_{is;js'}(\mathbf{k};\mathbf{G})$ the momentum $\mathbf{k}$ is the usual transmitted momentum. The second argument, $\mathbf{G}$, describes the non-conservation of the momentum due to presence of the superlattice: as expected, in a periodic structure the momentum must be conserved up to a reciprocal lattice vector $\mathbf{G}$. The latter condition is enforced by the delta-function $\delta_{\mathbf{G},\,\mathbf{k}_1+\mathbf{k}_2-\mathbf{k}'_1-\mathbf{k}'_2}$ in Eq. (S4). Thus, $U_{is;js'}(\mathbf{k};\mathbf{G})$ with $\mathbf{G} \neq 0$ corresponds to an umklapp scattering process.

Naturally, the interaction between electrons in the same layer differs from the interaction between electrons in different layers. Formally, for intralayer ($i = j$) interaction, one can separate the summation on $\mathbf{n}$ and $\mathbf{m}$ by the substitution $\mathbf{n} \to \mathbf{n} + \mathbf{m}$. As a result, we obtain

$$U_{is;is'}(\mathbf{k};\mathbf{G}) = \left(\sum_{\mathbf{b}^i} \delta_{\mathbf{b}^i,\mathbf{G}}\right) \sum_{\mathbf{n}} \exp(-i\mathbf{k}\mathbf{r}^i_{\mathbf{n}})\, U(\mathbf{r}^i_{\mathbf{n}} + \boldsymbol{\delta}^{is} - \boldsymbol{\delta}^{is'})\,, \tag{S5}$$

where the first and second summations are performed over all reciprocal lattice vectors ($\mathbf{b}^i$) and all lattice sites of the layer i, correspondingly. Let us introduce the symbol $\tilde{\mathbf{k}}^i = \tilde{\mathbf{k}}^i(\mathbf{k})$ to denote the vector $\mathbf{k}$ 'modulo' $\mathbf{b}^i$. Mathematically, it is

$$\tilde{\mathbf{k}}^i(\mathbf{k}) = \min_{\mathbf{b}^i}(\mathbf{k} - \mathbf{b}^i)\,. \tag{S6}$$

In other words, the vector $\tilde{\mathbf{k}}^i$ is the vector lying in the first Brillouin zone of the layer i, such that the difference $(\tilde{\mathbf{k}}^i - \mathbf{k})$ equals some reciprocal lattice vector $\mathbf{b}^i$. From equation (S5), we have $U_{is;is'}(\mathbf{k};\mathbf{G}) = U_{is;is'}(\tilde{\mathbf{k}}^i;\mathbf{G})$. Below we will use the continuum (low-$\mathbf{k}$) approximation for $U_{is;is'}(\mathbf{k};\mathbf{G})$, when one can replace the summation over lattice sites by the 2D integration. As a result, we obtain

$$U_{is;is'}(\mathbf{k};\mathbf{G}) = \frac{1}{\mathcal{V}_c}\left(\sum_{\mathbf{b}^i}\delta_{\mathbf{b}^i,\mathbf{G}}\right)\sum_{\mathbf{b}^i} U_{ii}(\mathbf{k}-\mathbf{b}^i)\,\exp[i(\mathbf{k}-\mathbf{b}^i)(\boldsymbol{\delta}^{is}-\boldsymbol{\delta}^{is'})] \approx \frac{1}{\mathcal{V}_c}U_{ii}(\tilde{\mathbf{k}}^i)\,\exp[i\tilde{\mathbf{k}}^i(\boldsymbol{\delta}^{is}-\boldsymbol{\delta}^{is'})]\sum_{\mathbf{b}^i}\delta_{\mathbf{b}^i,\mathbf{G}}\,, \tag{S7}$$

where $\mathcal{V}_c = \sqrt{3}a^2/2$ is the graphene unit cell area, and $U_{ii}(\mathbf{k}) = \int d^2r\, U(\mathbf{r})\, e^{-i\mathbf{k}\mathbf{r}}$ is the Fourier transform of the function $U(\mathbf{r})$.

We introduce also the Fourier transform for interlayer interaction as $U_{12}(\mathbf{k}) = \int d^2r\, U(d\mathbf{e}_z + \mathbf{r})\, e^{-i\mathbf{k}\mathbf{r}}$. Substituting this equation into Eq. (S4), one obtains

$$U_{1s;2s'}(\mathbf{k};\mathbf{G}) = \frac{1}{\mathcal{V}_c}\sum_{\mathbf{b}^1} U_{12}\left(\mathbf{k}+\mathbf{b}^1\right)\exp[i(\mathbf{k}+\mathbf{b}^1)(\boldsymbol{\delta}^{1s}-\boldsymbol{\delta}^{2s'})]\sum_{\mathbf{b}^2}\delta_{\mathbf{b}^2,\,\mathbf{b}^1+\mathbf{G}}\,. \tag{S8}$$

For the functions $U_{ij}(\mathbf{k})$, we use expressions for the screened Coulomb potential in the form [S1,S2]:

$$U_{ij}(\mathbf{q}) = \frac{v_{\mathbf{q}}}{1+\Pi_{\mathbf{q}}v_{\mathbf{q}}}\begin{pmatrix} 1 & e^{-qd} \\ e^{-qd} & 1 \end{pmatrix}. \tag{S9}$$

In this expression, the bare Coulomb potential is $v_{\mathbf{q}} = 2\pi e^2/\epsilon q$. The permittivity of the substrate is ϵ and $\Pi_{\mathbf{q}} \equiv -P(\omega = 0, \mathbf{q})$, where $P(\omega, \mathbf{q})$ is the polarization operator of the bilayer. In the low-$\mathbf{k}$ limit, we can keep a single term in the sum over $\mathbf{b}^1$ in Eq. (S8). The retained term corresponds to the smallest value of $|\mathbf{k} + \mathbf{b}^1|$. Formally, such $\mathbf{b}^1$ satisfies $\mathbf{k} + \mathbf{b}^1 = \tilde{\mathbf{k}}^1$. We already used this simplification to derive Eq. (S7). For Eq. (S8) this approximation works even better, since the interlayer potential $U_{12}(\mathbf{q})$ decays exponentially with q and $\exp(-|\mathbf{b}_{1,2}|d) \approx 5 \times 10^{-5}$. Below, we will use the long wavelength limit for the function $\Pi_{\mathbf{q}}$. In this case, it is independent of $\mathbf{q}$ and equals to the density of states of the bilayer at the Fermi level. We calculate the latter quantity numerically as described below.

Note that in some of our numerical calculations a more general form for the interaction function was used

$$U_{ij}(\mathbf{k}) \to U_{ij}(\mathbf{k}) + U_0\delta_{ij}\delta_{ss'}\delta_{\sigma\bar{\sigma}'}\,,$$

where $\bar{\sigma}$ means 'not σ'. The first term here is the screened Coulomb interaction, while the second one is purely local Hubbard interaction. Our numerical analysis shows that, as long as U_0 is not extremely large, it does not affect the obtained results. This is because the considered excitonic order couples electrons and holes, which mostly inhabit different layers. All results presented in the main text are obtained for $U_0 = 0$.

A. Effective interaction Hamiltonian

Projecting the full interaction Hamiltonian, Eq. (S4), onto the low-energy bands $\mathfrak{e}_\mu$ and $\mathfrak{h}_\mu$, we obtain the effective interaction Hamiltonian $H^{\text{eff}}_{\text{int}}$. Since the interaction is described by the product of four electron operators, even this truncated Hamiltonian will contain a large number of terms. Here we keep only those terms which affect the ordered phase at the mean-field level. Therefore, we obtain

$$\hat{H}^{\text{eff}}_{\text{int}} = \frac{1}{2\mathcal{N}}\sum_{\mathbf{pq}}\sum_{\mu\nu}\sum_{\sigma\sigma'}\left[A^{\mu\nu}_{\mathbf{pq}}\,\hat{\mathfrak{h}}^\dagger_{\mathbf{p}\mu\sigma}\,\hat{\mathfrak{h}}_{\mathbf{q}\nu\sigma}\,\hat{\mathfrak{e}}^\dagger_{\mathbf{q}\bar{\nu}\sigma'}\,\hat{\mathfrak{e}}_{\mathbf{p}\bar{\mu}\sigma'} + B^{\mu\nu}_{\mathbf{pq}}\,\hat{\mathfrak{h}}^\dagger_{\mathbf{p}\mu\sigma}\,\hat{\mathfrak{e}}_{\mathbf{q}\bar{\nu}\sigma}\,\hat{\mathfrak{h}}^\dagger_{\mathbf{q}\nu\sigma'}\,\hat{\mathfrak{e}}_{\mathbf{p}\bar{\mu}\sigma'} + \text{h.c.}\right], \tag{S10}$$

where $\bar{\mu} = -\mu$, and the projected coupling parameters are

$$A^{\mu\nu}_{\mathbf{pq}} = \sum_{\substack{is\\ js'}} \sum_{\substack{\mathbf{G}_1\mathbf{G}_2\\ \mathbf{G}'_1\mathbf{G}'_2}} \Phi^{\mathfrak{h}\mu *}_{\mathbf{pG}_1 is} \Phi^{\mathfrak{h}\nu}_{\mathbf{qG}'_1 is} \Phi^{\mathfrak{e}\bar{\nu} *}_{\mathbf{qG}_2 js'} \Phi^{\mathfrak{e}\bar{\mu}}_{\mathbf{pG}'_2 js'} U_{is;js'}(\mathbf{p}-\mathbf{q}+\mathbf{G}_1-\mathbf{G}'_1; \mathbf{G}_1+\mathbf{G}_2-\mathbf{G}'_1-\mathbf{G}'_2)\,, \tag{S11}$$

$$B^{\mu\nu}_{\mathbf{pq}} = \sum_{\substack{is\\ js'}} \sum_{\substack{\mathbf{G}_1\mathbf{G}_2\\ \mathbf{G}'_1\mathbf{G}'_2}} \Phi^{\mathfrak{h}\mu *}_{\mathbf{pG}_1 is} \Phi^{\mathfrak{e}\bar{\nu}}_{\mathbf{qG}'_1 is} \Phi^{\mathfrak{h}\nu *}_{\mathbf{qG}_2 js'} \Phi^{\mathfrak{e}\bar{\mu}}_{\mathbf{pG}'_2 js'} U_{is;js'}(\mathbf{p}-\mathbf{q}+\mathbf{G}_1-\mathbf{G}'_1; \mathbf{G}_1+\mathbf{G}_2-\mathbf{G}'_1-\mathbf{G}'_2)\,. \tag{S12}$$

For a given superstructure, bias voltage, and interaction strength, we calculate the functions $A^{\mu\nu}_{\mathbf{pq}}$ and $B^{\mu\nu}_{\mathbf{pq}}$ numerically. Our analysis shows that, with good accuracy, the following relations hold

$$A^{\mu\nu}_{\mathbf{pq}} \approx \delta_{\mu\nu} A_{\mathbf{pq}}\,, \qquad B^{\mu\nu}_{\mathbf{pq}} \approx \delta_{\mu\bar{\nu}} B_{\mathbf{pq}}\,. \tag{S13}$$

The deviations from these equalities do not exceed 1% for any of the superstructures considered. Note that in the limit of uncoupled graphene layers, $t_0 = 0$, Eqs. (S13) become exact. This follows from the symmetry of the wave functions $\Phi^{\mathfrak{e},\mathfrak{h}\mu}_{\mathbf{pG}is}$: for uncoupled layers the electrons are localized either in layer 1 or 2. Further, by choosing appropriate phases of $\Phi^{\mathfrak{e}\mu}_{\mathbf{pG}is}$ and $\Phi^{\mathfrak{h}\mu}_{\mathbf{pG}is}$, one can make $A_{\mathbf{pq}}$ and $B_{\mathbf{pq}}$ purely real. Numerical results demonstrate also that, if momenta $\mathbf{p}$ and $\mathbf{q}$ are located near the same Dirac point $\mathbf{K}_w$ (belonging to the same valley w), the functions $A_{\mathbf{pq}}$ and $B_{\mathbf{pq}}$ can be approximated as

$$A_{\mathbf{pq}} \approx \cos^2\!\left(\frac{\varphi_{\mathbf{p}} - \varphi_{\mathbf{q}}}{2}\right) U_{12}(\mathbf{p}-\mathbf{q})\,, \qquad B_{\mathbf{pq}} \approx \sin^2\!\left(\frac{\varphi_{\mathbf{p}} - \varphi_{\mathbf{q}}}{2}\right) U_{12}(\mathbf{p}-\mathbf{q})\,, \tag{S14}$$

where $\varphi_{\mathbf{p}}$ is the polar angle corresponding to the momentum $\mathbf{p}$ counted from the Dirac point $\mathbf{K}_w$. The factors $\cos^2[(\varphi_{\mathbf{p}} - \varphi_{\mathbf{q}})/2]$ and $\sin^2[(\varphi_{\mathbf{p}} - \varphi_{\mathbf{q}})/2]$ before the potential U_{12} are inherited from the wave functions. The deviation from equalities (S14) is larger for smaller θ. If $\mathbf{p}$ and $\mathbf{q}$ belong to different valleys, we have

$$A_{\mathbf{pq}} \approx 0\,, \quad B_{\mathbf{pq}} \approx 0\,. \tag{S15}$$

The latter equations demonstrate that, for interaction terms relevant to the formation of the excitonic order, the inter-valley scattering is suppressed. Thus, using these equations alongside with Eq. (S13), we can rewrite the effective interaction Hamiltonian in the form

$$\hat{H}^{\mathrm{eff}}_{\mathrm{int}} = \frac{1}{2\mathcal{N}} {\sum_{\mathbf{pq}}}' \sum_{\mu w} \sum_{\sigma\sigma'} \Big[A^w_{\mathbf{pq}}\, \hat{\mathfrak{h}}^{w\dagger}_{\mathbf{p}\mu\sigma}\, \hat{\mathfrak{h}}^{w}_{\mathbf{q}\mu\sigma}\, \hat{\mathfrak{e}}^{w\dagger}_{\mathbf{q}\bar{\mu}\sigma'}\, \hat{\mathfrak{e}}^{w}_{\mathbf{p}\bar{\mu}\sigma'} + B^w_{\mathbf{pq}}\, \hat{\mathfrak{h}}^{w\dagger}_{\mathbf{p}\mu\sigma}\, \hat{\mathfrak{e}}^{w}_{\mathbf{q}\mu\sigma}\, \hat{\mathfrak{h}}^{w\dagger}_{\mathbf{q}\bar{\mu}\sigma'}\, \hat{\mathfrak{e}}^{w}_{\mathbf{p}\bar{\mu}\sigma'} + \mathrm{h.c.} \Big]\,, \tag{S16}$$

where the electron operators $\hat{\mathfrak{h}}^w_{\mathbf{p}\mu\sigma}$ and $\hat{\mathfrak{e}}^w_{\mathbf{p}\mu\sigma}$ are given by Eq. (S2), the prime near the sum means that the summation is performed over momenta laying in one valley only, and $A^w_{\mathbf{pq}} = A_{\mathbf{K}_w+\mathbf{pK}_w+\mathbf{q}}$, $B^w_{\mathbf{pq}} = B_{\mathbf{K}_w+\mathbf{pK}_w+\mathbf{q}}$. Thus, the total effective Hamiltonian $H^{\mathrm{eff}} = H^{\mathrm{eff}}_0 + H^{\mathrm{eff}}_{\mathrm{int}}$ is diagonal in the valley index. This allows us to consider two valleys independently. Let us consider the valley around the Dirac point $\mathbf{K}_1$. Below we suppress the valley index and count the momenta from the Dirac point $\mathbf{K}_1$.

B. Mean-field equations

We now study the effective Hamiltonian in the mean-field approximation. To this end, we define the following symmetry-breaking expectation values

$$\eta_{\mathbf{p}\mu\sigma} = \langle \hat{\mathfrak{h}}^\dagger_{\mathbf{p}\mu\sigma} \hat{\mathfrak{e}}_{\mathbf{p}\bar{\mu}\bar{\sigma}} \rangle\,. \tag{S17}$$

The expectation value $\eta_{\mathbf{p}+1\sigma}$ couples electrons and holes belonging to the bands forming the Fermi surface, while the parameter $\eta_{\mathbf{p}-1\sigma}$ corresponds to the next pair of electron and hole bands (see Fig. S1). Note that the definition (S17) involves electrons and holes with opposite spin projections. Thus, this exciton order corresponds to the planar spin-density wave.

The matrix elements η's may be used in the usual mean-field decoupling scheme: a product of two operators O_1O_2 is replaced by a simpler expression according to the rule $O_1O_2 \to O_1\langle O_2\rangle + \langle O_1\rangle O_2 - \langle O_1\rangle\langle O_2\rangle$, where $\langle O_{1,2}\rangle \propto \eta_{\mathbf{p}\mu\sigma}$. Thus, $H^{\mathrm{eff}}_{\mathrm{int}}$ becomes quadratic in the $\hat{\mathfrak{e}}_{\mathbf{p}\mu\sigma}$ and $\hat{\mathfrak{h}}_{\mathbf{p}\mu\sigma}$ operators. Let us now introduce the following four-component operator $\hat{\Psi}_{\mathbf{p}\mu} = (\hat{\mathfrak{h}}_{\mathbf{p}\mu\uparrow}, \hat{\mathfrak{e}}_{\mathbf{p}\bar{\mu}\uparrow}, \hat{\mathfrak{h}}_{\mathbf{p}\mu\downarrow}, \hat{\mathfrak{e}}_{\mathbf{p}\bar{\mu}\downarrow})^{\mathrm{T}}$. The effective mean-field Hamiltonian can then be written in the form

$$\hat{H}^{\mathrm{eff}}_{\mathrm{MF}} = \sum_{\mathbf{p}\mu} \hat{\Psi}^\dagger_{\mathbf{p}\mu} H_{\mathbf{p}\mu} \hat{\Psi}_{\mathbf{p}\mu} + U_c\,, \tag{S18}$$

where U_c is the c-number

$$U_c = \frac{1}{2\mathcal{N}} \sum_{\mathbf{pq}\mu\sigma} \left[A_{\mathbf{pq}}\, \eta^*_{\mathbf{p}\mu\sigma}\, \eta_{\mathbf{q}\mu\sigma} + B_{\mathbf{pq}}\, \eta^*_{\mathbf{p}\mu\sigma}\, \eta^*_{\mathbf{q}\mu\bar{\sigma}} + \text{c.c.} \right]. \tag{S19}$$

In equation (S18), $H_{\mathbf{p}\mu}$ is a 4×4 matrix, which has the form

$$H_{\mathbf{p}\mu} = \begin{pmatrix} E^{\mathfrak{h}}_{\mathbf{p}\mu} & 0 & 0 & -\Delta^*_{\mathbf{p}\mu\uparrow} \\ 0 & E^{\mathfrak{e}}_{\mathbf{p}\mu} & -\Delta_{\mathbf{p}\mu\downarrow} & 0 \\ 0 & -\Delta^*_{\mathbf{p}\mu\downarrow} & E^{\mathfrak{h}}_{\mathbf{p}\mu} & 0 \\ -\Delta_{\mathbf{p}\mu\uparrow} & 0 & 0 & E^{\mathfrak{e}}_{\mathbf{p}\mu} \end{pmatrix}, \tag{S20}$$

where $\Delta_{\mathbf{p}\mu\sigma}$ is the order parameter

$$\Delta_{\mathbf{p}\mu\sigma} = \frac{1}{\mathcal{N}} \sum_{\mathbf{q}} \left[A_{\mathbf{pq}}\, \eta_{\mathbf{q}\mu\sigma} + B_{\mathbf{pq}}\, \eta^*_{\mathbf{q}\mu\bar{\sigma}} \right]. \tag{S21}$$

Note that, in principle, one can introduce also the expectation values of the form $\langle \hat{\mathfrak{h}}^\dagger_{\mathbf{p}\mu\sigma} \hat{\mathfrak{e}}_{\mathbf{p}\mu\bar{\sigma}} \rangle$ making effective mean-field Hamiltonian non-diagonal in terms of index μ. However, the corresponding interaction constants turn out to be much smaller than functions $A_{\mathbf{pq}}$ and $B_{\mathbf{pq}}$. Thus, we neglect these order parameters. Finally, the charge-density-wave state represented by order parameter $\sum_\sigma \langle \hat{\mathfrak{h}}^{w\dagger}_{\mathbf{p}\mu\sigma} \hat{\mathfrak{e}}^{w}_{\mathbf{p}\bar{\mu}\sigma} \rangle$ is energetically unfavorable in comparison to the SDW one.

We now assume that $\Delta_{\mathbf{p}\mu\sigma}$ are real-valued functions satisfying the relations $\Delta_{\mathbf{p}\mu\uparrow} = \Delta_{\mathbf{p}\mu\downarrow} \equiv \Delta_{\mathbf{p}\mu}$. Minimizing the total energy, at zero temperature and at half-filling, we obtain the system of equations for the order parameters:

$$\Delta_{\mathbf{p}\mu} = \frac{1}{2} \int \frac{d^2q}{v_{\text{BZ}}} \left[\frac{A_{\mathbf{pq}} \Delta_{\mathbf{q}\mu}}{\sqrt{\Delta^2_{\mathbf{q}\mu} + E^2_{\mathbf{q}\mu}}} + \frac{B_{\mathbf{pq}} \Delta_{\mathbf{q}\bar{\mu}}}{\sqrt{\Delta^2_{\mathbf{q}\bar{\mu}} + E^2_{\mathbf{q}\bar{\mu}}}} \right], \tag{S22}$$

where $E_{\mathbf{p}\mu} = (E^{\mathfrak{e}}_{\mathbf{p}\bar{\mu}} - E^{\mathfrak{h}}_{\mathbf{p}\mu})/2$, $v_{\text{BZ}} = 8\pi^2/(a^2\sqrt{3})$ is the area of the graphene Brillouin zone (BZ), and the integration is performed over the momenta laying in one valley.

II. APPROXIMATE MEAN-FIELD EQUATIONS

Equations (S22) are the system of integral equations for the gap functions $\Delta_{\mathbf{p}+1}$ and $\Delta_{\mathbf{p}-1}$. One can find approximate solutions to these equations assuming an appropriate ansatz for the gap functions $\Delta_{\mathbf{p}\mu}$. In this section, we derive approximate transcendental equations for these order parameters assuming a step-like form for the functions $\Delta_{\mathbf{p}\mu}$. These equations will be different for weak and strong interaction strength. The criterion that distinguishes the strong interaction from the weak one will be given below.

A. Weak-interaction limit

The main interest now is the value of the function $\Delta_{\mathbf{p}+1}$ at the Fermi surface, since this provides the energy gap. The Fermi surface near each Dirac point is a closed curve having near-circular shape. Below we neglect the trigonal warping and approximate the Fermi surface by a circle with radius q^*_F, calculated numerically by averaging over the Fermi surface. We assume that $\Delta_{\mathbf{p}\mu}$ are step-like functions, described by the equations

$$\Delta_{\mathbf{p}\mu} = \Delta_\mu \Theta(q_\Lambda - |p - q^*_F|), \tag{S23}$$

where the cutoff momentum q_Λ will be specified below. Thus, if $q_\Lambda < q^*_F$, the region of integration in Eq. (S22) is a ring centered at the Dirac point $\mathbf{K}_1$ and having radii $(q^*_F - q_\Lambda)$ and $(q^*_F + q_\Lambda)$. Otherwise, when $q_\Lambda > q^*_F$, it is the circle with radius $(q^*_F + q_\Lambda)$.

In a subsequent approximation, we replace the functions $A_{\mathbf{pq}}$ and $B_{\mathbf{pq}}$ by constants $\bar{A}$ and $\bar{B}$, obtained by averaging $A_{\mathbf{pq}}$ and $B_{\mathbf{pq}}$ over the Fermi surface. For numerical calculations of $\bar{A}$ and $\bar{B}$, we consider $A_{\mathbf{pq}} = \sum_\mu A^{\mu\mu}_{\mathbf{pq}}/2$ and $B_{\mathbf{pq}} = \sum_\mu B^{\mu\bar{\mu}}_{\mathbf{pq}}/2$, with $A^{\mu\nu}_{\mathbf{pq}}$ and $B^{\mu\nu}_{\mathbf{pq}}$ calculated according to Eqs. (S12).

We now also approximate the energies $E_{\mathbf{q}\mu}$ by linear functions

$$E_{\mathbf{q}\mu} \approx v^*_{\text{F}}(|\mathbf{q}| - \mu q^*_F), \tag{S24}$$

where the renormalized Fermi velocity is calculated numerically by averaging the function $\sum_\mu |\partial E_{\mathbf{q}\mu}\partial \mathbf{q}|/2$ over the Fermi surface. Thus, the system of equations for the order parameters becomes

$$\Delta_\mu = \frac{1}{2}\int\limits_{q_1}^{q_2} dq \left[\frac{q\lambda_A \Delta_\mu}{\sqrt{\Delta_\mu^2 + v_{\rm F}^{*2}(q-\mu q_F^*)^2}} + \frac{q\lambda_B \Delta_{\bar\mu}}{\sqrt{\Delta_{\bar\mu}^2 + v_{\rm F}^{*2}(q+\mu q_F^*)^2}} \right], \tag{S25}$$

where $q_1 = \max(0,\, q_F^* - q_\Lambda)$, and $q_2 = q_F^* + q_\Lambda$. The interaction parameters are $\lambda_A = 2\pi\bar{A}/v_{\rm BZ}$ and $\lambda_B = 2\pi\bar{B}/v_{\rm BZ}$. The magnitude of the order parameters Δ_μ depends on the values of $\bar{A}$ and $\bar{B}$, as well as on the cut-off momentum q_Λ. The main contribution to the functions $A_{\mathbf{pq}}$ and $B_{\mathbf{pq}}$ comes from the interlayer interaction [see Eq. (S14)]. Following Refs. [S1,S2], we define q_Λ from the condition $U_{12}(q_\Lambda) = U_{12}(0)/2$. Assuming that $q_\Lambda d \ll 1$ (which is correct for $V_b \lesssim t_0$ and $e^2/\epsilon v_{\rm F} \lesssim 1$), from Eqs. (S9) we obtain the estimate $q_\Lambda \approx 2\pi\Pi_0 v_{\rm F}\alpha$, where Π_0 is the density of states of the bilayer at the Fermi level, $\alpha = e^2/\epsilon v_{\rm F}$ is the graphene fine structure constant, and $v_{\rm F} = ta\sqrt{3}/2$ is the Fermi velocity of the single-layer graphene. Neglecting the trigonal warping, the density of states is expressed as $\Pi_0 \approx 4q_F^*/(\pi v_{\rm F}^*)$. Thus, we obtain

$$q_\Lambda = 8\frac{v_{\rm F}}{v_{\rm F}^*}\alpha q_F^*\,. \tag{S26}$$

The integrals in Eq. (S25) can be evaluated explicitly. Performing the integration, we derive the system of transcendental equations for the parameters Δ_μ. Assuming that $q_\lambda \ll q_F^*$ and $\Delta_\mu \ll V_b$, one can solve the system of equations (S25) analytically. This gives

$$\Delta_{+1} \;\approx\; 2\, v_{\rm F}\, q_F^*\, \alpha\, \exp(-1/\Lambda + 4\alpha^*), \qquad \Delta_{-1} = \frac{\bar{B}}{\bar{A}}\Delta_{+1}\,, \tag{S27}$$

where $\alpha^* = e^2/(\epsilon v_{\rm F}^*)$ is the 'renormalized α' and

$$\Lambda \approx \frac{2\pi\bar{A}\, q_F^*}{v_{\rm BZ} v_{\rm F}^*}\,. \tag{S28}$$

Using the approximation (S14) for $A_{\mathbf{pq}}$, we obtain

$$\bar{A} \approx \left\langle \cos^2\!\Big(\varphi/2\Big)\, U_{12}\Big(2q_F^*|\sin(\varphi/2)|\Big)\right\rangle, \tag{S29}$$

where φ is the polar angle parameterizing points on the Fermi surface, while the averaging is performed over this angle. Substituting this expression into Eq. (S28), we obtain

$$\Lambda \approx \frac{1}{8}\left\langle \frac{\cos^2(\varphi/2)}{1 + \dfrac{1}{4\alpha^*}|\sin(\varphi/2)|} \right\rangle. \tag{S30}$$

Deriving the above approximation, we assumed that $q_F^* d \ll 1$, which is valid for all bias voltages considered. According to Eq. (S30), the parameter Λ increases when α^* increases. When $\alpha^* \ll 1$, we have $\Lambda \propto \alpha^* \ln(1/\alpha^*)$. Since α^* is inversely proportional to $v_{\rm F}^*$, the quantity Λ and, consequently, Δ_{+1} increases when $v_{\rm F}^*$ decreases. Therefore, the order parameter Δ_{+1} increases with θ, because $v_{\rm F}^*$ decreases with the twist angle [S3,S4,S5]. Numerical calculations also show that the actual value of $\bar{A}$ is greater than the estimate (S29). This can be explained by the fact that at finite interlayer hybridization, the quasiparticles are no longer localized in one particular layer. As a result, the intralayer potential contributes to $\bar{A}$, and this effect is stronger for smaller twist angles.

B. Approximate solution, strong interaction limit

The limit of weak coupling corresponds to the case of $\alpha \ll 1$. Simple estimates show, however, that for a bilayer suspended in vacuum, $\epsilon = 1$, the parameter $\alpha \approx 2.6$. When α increases, the cut-off momentum can exceed the size of the superlattice Brillouin zone. In this case, we should increase the number of bands in our effective Hamiltonian. Simultaneously, we should increase the number of order parameters $\Delta_{\mathbf{p}\mu}$, with μ now changing from 1 to some $N > 2$. The rank of the matrix functions $A^{\mu\nu}$ and $B^{\mu\nu}$ becomes equal to N. This consideration can be substantially simplified if we consider the additional 'high-energy' bands in the limit of decoupled ($t_0 = 0$) graphene layers. The decoupled layer approximation is justified for sufficiently large energies. Due to its importance, let us discuss this approximation in some detail.

1. Decoupled layer approximation

Imagine that we have no interlayer hopping. In such a situation the tBLG single-electron spectrum coincides with the spectrum of two graphene layers folded inside the tBLG superlattice Brillouin zone. As the interlayer coupling increases, this spectrum changes as well. One of the well-known features which emerges at finite interlayer hopping is a series of van Hove singularities at finite energies $\pm E_{\rm vH}^{(u)}$, where the integer super-index u orders the singularities linearly: $E_{\rm vH}^{(u+1)} > E_{\rm vH}^{(u)}$. In the limit of vanishing interlayer hopping, the singularity energies may be estimated with the help of perturbation theory in t_0. Exactly at $t_0 = 0$, the tBLG spectrum has multiple degeneracy lines defined by the condition:

$$v_{\rm F}|\mathbf{k}+\mathbf{K}_1| = v_{\rm F}|\mathbf{k}+\mathbf{K}_2+\mathbf{G}|\,, \quad \text{where} \quad \mathbf{G} = n\boldsymbol{\mathcal{G}}_1 + m\boldsymbol{\mathcal{G}}_2, \quad n,\ m \quad \text{are integers}\,. \tag{S31}$$

This relation equates electron energies in different layers at different valleys. The momentum conservation is enforced up to a reciprocal superlattice vector $\mathbf{G}$. It is convenient to rewrite Eq. (S31) as

$$v_{\rm F}|\mathbf{k}| = v_{\rm F}|\mathbf{k}+\mathbf{G}'|\,, \quad \text{where} \quad \mathbf{G}' = \mathbf{G}+\mathbf{K}_2-\mathbf{K}_1 = (n+1/3)\boldsymbol{\mathcal{G}}_1 + (m-1/3)\boldsymbol{\mathcal{G}}_2\,. \tag{S32}$$

The solution of this equation is a straight line defined by the formula $\mathbf{k} = -\mathbf{G}'/2 + \mathbf{p}_0\ell$, where ℓ is a scalar variable and the vector $\mathbf{p}_0$ is normal to $\mathbf{G}'$, that is $(\mathbf{p}_0\cdot\mathbf{G}') = 0$. The energy corresponding to the degenerate states is equal to

$$E^{(0)} = v_{\rm F}\sqrt{(\mathbf{G}'/2)^2 + \mathbf{p}_0^2\ell^2}. \tag{S33}$$

At small, but finite, tunneling, these degeneracies are lifted as follows: $E_\pm = E^{(0)} \pm \Delta E^{(1)}$, where the correction $\Delta E^{(1)}$ is proportional to $|t_0|$. When this degeneracy is lifted, the van Hove singularity appears. They are approximately located at $\partial E^{(0)}/\partial\ell = 0$, or, equivalently, at $E_{\rm vH} \approx v_{\rm F}|\mathbf{G}'|$.

However, despite the importance of the van Hove singularities for general properties of solids, for us the renormalization of the low-energy spectrum ($|\varepsilon| < E_{\rm vH}^{(1)}$) is more relevant. The feature we are specifically interested in is the renormalized Fermi velocity $v_{\rm F}^* < v_{\rm F}$. Both, the first van Hove singularity and the low-energy renormalizations are due to the interlayer hybridization amplitudes $\tilde{t}_{12}^{ss'}(\mathbf{k};\mathbf{G})|_{\mathbf{G}=0}$, $\tilde{t}_{12}^{ss'}(\mathbf{k};\mathbf{G})|_{\mathbf{G}=-\boldsymbol{\mathcal{G}}_1}$, and $\tilde{t}_{12}^{ss'}(\mathbf{k};\mathbf{G})|_{\mathbf{G}=\boldsymbol{\mathcal{G}}_2}$. These three choices for the momentum $\mathbf{G}$ correspond to the lowest value of the parameter $G' = |\mathbf{G}'|$: for such values of $\mathbf{G}$ one can calculate $G' = G'_{\rm min} = |\boldsymbol{\mathcal{G}}_1|/\sqrt{3}$. For all other choices of $\mathbf{G}$, the following inequality is valid: $G' \geq 2G'_{\rm min}$. As it was demonstrated in Ref. [S6], the tunneling amplitude $\tilde{t}_{12}^{ss'}(\mathbf{k};\mathbf{G})$ is very sensitive to the value of G': it decays quickly for larger G'. Thus, we neglect the interlayer tunneling for single-electron states with momentum $|\mathbf{q}| > |\boldsymbol{\mathcal{G}}_{1,2}|$, and approximate these states by wave functions localized inside an individual layer.

2. Derivation of the strong coupling equations

Using the decoupled-layer approximation we will now derive the strong-coupling equations. Our formal goal now is to modify Eq. (S22) to account for momenta $q \gtrsim |\boldsymbol{\mathcal{G}}_1|$. For decoupled layers, one can associate the band index S to the momentum $\mathbf{p}$ laying in the Brillouin zone of the layer 1 or 2; that is, one can perform the band unfolding [S7]. Therefore, one can assume that the number of order parameters $\Delta_{\mathbf{p}\mu}$ is still equal to 2, but the integration in Eq. (S22) is extended to momenta exceeding $q_0 = |\boldsymbol{\mathcal{G}}_{1,2}|/(2\sqrt{3})$.

To complete the procedure, we need an approximation for $E_{\mathbf{q}\mu}$ for $q > q_0$. Applying the decoupled-layer approach, we write

$$E_{\mathbf{q}+1} \approx E_{\mathbf{q}-1} \approx v_{\rm F}|\mathbf{q}|\,. \tag{S34}$$

This expression assumes that at high energies: (i) one must use the non-renormalized Fermi velocity $v_{\rm F}$, and (ii) the bias voltage may be neglected, since $V_b \lesssim t_0$. Equation (S34) supplements Eq. (S24) at higher momenta. Therefore, approximate equations for the order parameters Δ_μ become

$$\Delta_\mu = \int_0^{q_0} dq \frac{\frac{1}{2}q\lambda_A\Delta_\mu}{\sqrt{\Delta_\mu^2 + v_{\rm F}^{*2}(q-\mu q_F^*)^2}} + \int_{q_0}^{q_\Lambda} dq \frac{\frac{1}{2}q\lambda_A\Delta_\mu}{\sqrt{\Delta_\mu^2 + v_{\rm F}^2 q^2}} + \int_0^{q_0} dq \frac{\frac{1}{2}q\lambda_B\Delta_{\bar\mu}}{\sqrt{\Delta_{\bar\mu}^2 + v_{\rm F}^{*2}(q+\mu q_F^*)^2}} + \int_{q_0}^{q_\Lambda} dq \frac{\frac{1}{2}q\lambda_B\Delta_{\bar\mu}}{\sqrt{\Delta_{\bar\mu}^2 + v_{\rm F}^2 q^2}}\,. \tag{S35}$$

Similarly to Eq. (S25), integrals here can be evaluated explicitly, and, thus, we obtain the system of transcendental equations for the parameters Δ_μ.

Finally, we note that even in the strong-coupling regime, the two valleys should be still considered independently. In other words, there is no coupling between the order parameters in different valleys. To understand why this is the case, it is useful to re-examine the formalism in the unfolded Brillouin zone. Layer 1 has two non-equivalent Dirac points, $\mathbf{K}$ and $\mathbf{K}'$ $(= -\mathbf{K})$. A rotation by the twist angle θ transforms $\mathbf{K}$ and $\mathbf{K}'$ into the layer-2 Dirac points, $\mathbf{K}_\theta$ and $\mathbf{K}'_\theta$ $(= -\mathbf{K}_\theta)$. The order parameter we study in this work describes the condensation of the electron-hole pairs which are composed of an electron with momentum $(\mathbf{K}+\mathbf{p})$ and a hole with momentum $(\mathbf{K}'_\theta+\mathbf{p})$ (valley 1), or an electron with momentum $(\mathbf{K}'+\mathbf{p}')$ and a hole with momentum $(\mathbf{K}_\theta+\mathbf{p}')$ (valley 2) [S8]. Let us denote by $\hat{\mathfrak{e}}_{\mathbf{K}+\mathbf{p}\sigma}$ and $\hat{\mathfrak{h}}_{\mathbf{K}'_\theta+\mathbf{p}\sigma}$ the corresponding electron and hole operators in valley 1, and by $\hat{\mathfrak{e}}_{\mathbf{K}'+\mathbf{p}'\sigma}$ and $\hat{\mathfrak{h}}_{\mathbf{K}_\theta+\mathbf{p}'\sigma}$ the electron and hole operators in valley 2. For simplicity, only bands crossing the Fermi level are considered. There are two terms which may couple the order parameter in different valleys. One of them is proportional to

$$-\tilde{U}_1(\mathbf{Q})\,\hat{\mathfrak{e}}^\dagger_{\mathbf{K}+\mathbf{p}\sigma}\,\hat{\mathfrak{h}}_{\mathbf{K}'_\theta+\mathbf{p}\bar{\sigma}}\,\hat{\mathfrak{e}}^\dagger_{\mathbf{K}'+\mathbf{p}'\bar{\sigma}}\,\hat{\mathfrak{h}}_{\mathbf{K}_\theta+\mathbf{p}'\sigma}+\text{h.c.} \tag{S36}$$

The quantity $\tilde{U}_1 > 0$ is the effective coupling constant in this channel. It depends on the transfer momentum $\mathbf{Q} = \mathbf{K} - \mathbf{K}_\theta + \mathbf{p} - \mathbf{p}'$. The contribution of this term to the mean-field energy is $\sim (\eta^w \eta^{w'} + \text{c.c.})$, where the valley indices w and w' are unequal: $w \neq w'$. Another term

$$-\tilde{U}_2(\mathbf{Q})\,\hat{\mathfrak{e}}^\dagger_{\mathbf{K}+\mathbf{p}\sigma}\,\hat{\mathfrak{h}}_{\mathbf{K}'_\theta+\mathbf{p}\bar{\sigma}}\,\hat{\mathfrak{h}}^\dagger_{\mathbf{K}_\theta+\mathbf{p}'\bar{\sigma}}\,\hat{\mathfrak{e}}_{\mathbf{K}'+\mathbf{p}'\sigma}+\text{h.c.}\,, \tag{S37}$$

with transfer momentum $\mathbf{Q} = \mathbf{K}-\mathbf{K}'+\mathbf{p}-\mathbf{p}'$, and its own effective coupling constant $\tilde{U}_2 > 0$, generates a contribution $\sim [\eta^w(\eta^{w'})^* + \text{c.c.}]$, where $w \neq w'$. Although this term does not conserve momentum, for commensurate angles it is allowed due to the presence of the superlattice: the non-conserved momentum $\Delta\mathbf{K}_{\text{tot}}$ is a reciprocal superlattice vector, $\Delta\mathbf{K}_{\text{tot}} = 2(\mathbf{K}+\mathbf{K}_\theta) = 2(2m_0+r)\boldsymbol{\mathcal{G}}_2 \sim 0$ [S9].

The effective inter-valley interaction constants $\tilde{U}_{1,2}$ are obtained by projection of the bare interaction, Eq. (S9), on the $\mathfrak{e}$ and $\mathfrak{h}$ bands, as explained above. In the limit of uncoupled layers, the electrons and the holes exist in different layers. Thus, $\tilde{U}_1$ will be strictly zero. For $\tilde{U}_2$ we can write $\tilde{U}_2 \sim U_{12}(\mathbf{Q})$. Since for this term the transfer momentum is large, $\mathbf{Q} = \mathbf{K} - \mathbf{K}' + \mathbf{p} - \mathbf{p}' \sim 2\mathbf{K} \sim \mathbf{b}_{1,2}$, the term (S37) will be negligible due to the exponent in $U_{12}(\mathbf{Q})$, see Eq. (S9). For finite inter-layer hybridization, $\tilde{U}_1$ will be non-zero. Likewise, the value of $\tilde{U}_2$ will be larger than that for uncoupled layers. Our numerical analysis shows, however, that the inter-valley interaction is much smaller than the intra-valley one for any superstructures and model parameters studied. The above analysis allows the derivation of Eq. (S15). A similar considerations can be done for the upper bands, not forming the Fermi surface. Thus, we can neglect the inter-valley scattering.

[S1] Y.E. Lozovik and A. Sokolik, "Electron-hole pair condensation in a graphene bilayer," JETP letters **87**, 55 (2008).

[S2] Y.E. Lozovik and A. Sokolik, "Multi-band pairing of ultrarelativistic electrons and holes in graphene bilayer," Physics Letters A **374**, 326 (2009).

[S3] J.M.B. Lopes dos Santos, N.M.R. Peres, and A.H. Castro Neto, "Graphene Bilayer with a Twist: Electronic Structure," Phys. Rev. Lett. **99**, 256802 (2007).

[S4] R. Bistritzer and A.H. MacDonald, "Moiré bands in twisted double-layer graphene," Proceedings of the National Academy of Sciences **108**, 12233 (2011).

[S5] A.O. Sboychakov, A.L. Rakhmanov, A.V. Rozhkov, and F. Nori, "Electronic spectrum of twisted bilayer graphene," Phys. Rev. B **92**, 075402 (2015).

[S6] J.M.B. Lopes dos Santos, N.M.R. Peres, and A.H. Castro Neto, "Continuum model of the twisted graphene bilayer," Phys. Rev. B **86**, 155449 (2012).

[S7] H. Nishi, Y.-i. Matsushita, and A. Oshiyama, "Band-unfolding approach to Moiré-induced band-gap opening and Fermi level velocity reduction in twisted bilayer graphene," Phys. Rev. B **95**, 085420 (2017).

[S8] For superstructures with $r \neq 3n$. Otherwise, the electron and the hole have momenta $\mathbf{K}+\mathbf{p}$ and $\mathbf{K}_\theta+\mathbf{p}$, respectively, in valley 1, and $\mathbf{K}'+\mathbf{p}'$ and $\mathbf{K}'_\theta+\mathbf{p}'$ in valley 2.

[S9] This formula is written for $r \neq 3n$. It can be easily shown that the expression $\Delta\mathbf{K}_{\text{tot}} \sim 0$ is valid also for $r = 3n$.